Aquatic Geochemistry (2005) 11:413–431
DOI 10.1007/s10498-005-7441-2

Phase Transformations and Proton Promoted Dissolution of Hydrous Manganite (γ-MnOOH)

MADELEINE RAMSTEDT[1,2] and STAFFAN SJÖBERG[1]
[1]*Department of Chemistry, Inorganic chemistry, Umeå University, SE-901 87, Umeå, Sweden;*
[2]*STI-IMX-LMCH, EPFL, Station 12, CH-1015, Lausanne, Switzerland*

(Received 2 December 2004; accepted 11 May 2005)

Abstract. The objective of this study was to describe the proton promoted disproportion of synthetic manganite (γ-MnOOH) and to characterise the resulting phase transformations. The solution and remaining solid phase after disproportionation was analysed by techniques including atomic absorbance spectroscopy, X-ray diffraction (XRD), atomic force microscopy (AFM) and scanning electron microscopy (SEM). In suspensions with pH between 5 and 7, $-\log[H^+]$ was monitored for 17 months and equilibrium constants were determined at 9, 12 and 17 months of reaction time for the following reaction (25 °C, 0.1 M (Na)NO_3):

$$2\gamma\text{-MnOOH} + 2H^+ \rightleftharpoons MnO_2 + Mn^{2+} + 2H_2O$$

The formed MnO_2 ages with time and the equilibrium constant for a metastable phase (ramsdellite or nsutite) as well as the most stable phase, pyrolusite (β-MnO_2), was determined. Furthermore, combined pH and pe (Eh) measurements were performed to study the equilibrium;

$$\gamma\text{-MnOOH(s)} \rightleftharpoons \beta\text{-}MnO_2(s) + H^+ + e^-$$

Real-time AFM measurements of the dissolution showed shrinkage of the length of the manganite needles with time (2 hours). After 1 week SEM images showed that this decreased length also was followed by a reduced thickness of the manganite needles. From the SEM images the morphology of the formed Mn(IV) oxides was studied. At pH 2.6, pyrolusite (β-MnO_2) and $MnCl_2$ were found in the XRD patterns. Throughout the pH range there were indications of ramsdellite ($MnO_{1.97}$) in the XRD patterns, which coincided with the existence of a fraction of needle shaped crystals with smaller dimensions (compared to manganite) in the SEM images. These observations together with the long term dissolution experiments suggest that the dissolution of manganite initially forms a ramsdellite or nsutite phase that over time rearranges to form pyrolusite.

Key words: manganite, gamma-MnOOH, disproportionation, dissolution, pyrolusite, MnO_2, AFM, XRD, SEM, phase transformation

1. Introduction

Mineral surfaces are important in environmental processes where they regulate mobility and speciation of metals and inorganic/organic ligands. Many minerals dissolve through redox processes and, consequently, can play an

important role in the environmental cycling of redox active elements. In the literature many examples can be found of these processes with manganese oxides for example reductive dissolution of manganite in the presence of As(III) and Cr(III) (Chiu and Hering, 2000; Johnson and Xyla, 1991; Weaver et al., 2002) or organic substances such as oxalate (Xyla et al., 1992) and aminocarboxylates (Mcardell et al., 1998). Furthermore, these redox reactions can increase the toxicity of substances such as Cr(III) (Weaver et al., 2002) and affect the mobility of nuclides such as Pu(VI) (Shaughnessy et al., 2003).

In oxygen containing lake waters, manganese can be oxidised and form manganite (γ-MnOOH) (Hem et al., 1983; Stumm and Giovanoli 1976; Murray et al., 1985), which is the most stable trivalent manganese hydroxide (Varentsov and Grassely, 1980). Due to the trivalent state of manganese, manganite has the ability to act both as a reducing and oxidizing agent. It has been shown that trivalent manganese forms the most reactive sites in manganese minerals with mixed valence (Manceau et al., 1997; Nico et al., 2001). This suggests that manganite also could be used as a model substance for the reactivity of trivalent manganese in other minerals. As a consequence, manganite is an important mineral in the understanding, modelling and prediction of environmental processes.

Previous observations show that manganite significantly dissolves below pH 6 (Bochatay et al., 2000; Ramstedt et al., 2002). In the literature, the dissolution process of trivalent manganese oxides is commonly described as a disproportionation reaction (1) forming soluble Mn^{2+} and MnO_2(s) (Bricker, 1965; Klewicki and Morgan, 1999).

$$2MnOOH(s) + 2H^+ \rightleftharpoons MnO_2(s) + Mn^{2+} + 2H_2O \quad (1)$$

Depending on the experimental conditions different polymorphs of Mn(IV)-oxide can be formed. Previous studies show that oxidation/dissolution of hausmannite and other MnOOH polymorphs can form non-stoichiometric MnO_2(s) (Bricker, 1965), birnessite (δ-$MnO_{1.8}$) (Bricker, 1965; Varentsov and Grasselly, 1980), nsutite (γ-$MnO_{1.9}$) (Bricker, 1965) ramsdellite (MnO_2) (Kohler et al., 1997; Yamada and Ohmasa, 1986) and/or pyrolusite (β-MnO_2) (Amouric et al., 1991; Giovanoli and Leuenberger, 1969; Varentsov and Grassely, 1980; Yamada and Ohmasa 1986). The structure of these $Mn^{IV}O_2$ phases varies from sheet like structure in birnessite (Figure 1) to small sized tunnel structures in ramsdellite, nsutite and pyrolusite (Post, 1999). The nsutite phase can be described as an intergrowth of the ramsdellite and pyrolusite phase with regions of the different characteristic tunnel sizes alternating throughout the structure (Chabre and Pannetier, 1995).

The study by Bricker (1965) provides a careful characterization of the stability relations among the different manganese oxides. The Mn^{2+}/

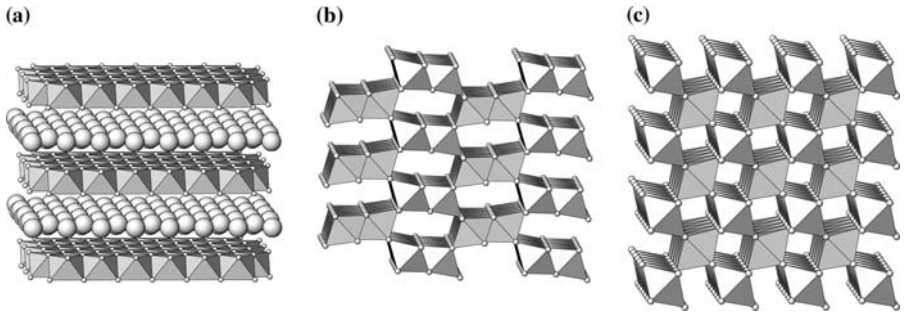

Figure 1. The structures of (a) birnessite, (b) ramsdellite and (c) pyrolusite. The MnO_6 octahedra are arranged in tunnel and sheet like structures. In birnessite, counter ions are found between the sheets to balance the charge formed by replacement of Mn^{IV} in the structure by Mn^{III} and Mn^{II}.

γ-MnOOH boundary was studied at known activities of Mn^{2+} within the pH range 6.4–7.0. Stable potentials with respect to pH and Eh were obtained within a few days and resulted in log K(2) = 25.35 ($E^0 = 1.500$ V).

$$\gamma - \mathrm{MnOOH} + 3\mathrm{H}^+ + \mathrm{e}^- \rightleftharpoons \mathrm{Mn}^{2+} + 2\mathrm{H_2O} \quad (2)$$

Corresponding measurements were performed to determine the stability of δ-MnO_2, (birnessite) and γ-MnO_2 (nsutite) as defined by the reaction

$$\mathrm{MnO_2} + 4\mathrm{H}^+ + 2\mathrm{e}^- \rightleftharpoons \mathrm{Mn}^{2+} + 2\mathrm{H_2O} \quad (3)$$

The obtained results were: log K(3)(δ-$MnO_{1.8}$) = 34.92 ($E^0 = 1.291$ V) and log K(3)(γ-$MnO_{1.9}$) = 38.73 ($E^0 = 1.273$ V). No attempts were made by Bricker to study the Mn^{2+}/β-MnO_2 (pyrolusite) boundary. However, pyrolusite is the most stable phase of MnO_2 and a number of studies of the corresponding standard potential of (3) are found in the literature (Högfeldt, 1982; Sillén and Martell, 1971). Ambrose et al. (1969) compared E^0 values of variously prepared and treated samples of pyrolusite and found values between 1.195 V (logK(3) = 40.28) and 1.244 V (log K(3) = 40.92). The lowest standard potentials were shown by the most highly crystalline samples and those being the most stoichiometric. By combining reactions (2) and (3), the disproportionation reaction (1) is obtained. Direct studies of this phase transformation along the MnOOH/MnO_2 boundary have not been published earlier. Klewecki and Morgan (1999) report a value of log K(1) $\approx$7.0 with very few details related to experimental design, equilibrium times and ageing effects.

To further an understanding of the complex dissolution/disproportionation process (1), a number of dissolution experiments were performed. Long term phase transformations were followed in suspensions consisting of

crystalline nanosized manganite particles by measuring pH, Eh (pe) and [Mn^{2+}]. Furthermore, combined pH and pe measurements made it possible to study the equilibrium (4).

$$MnO_2 + H^+ + e^- \rightleftharpoons MnOOH \quad (4)$$

Also, short term phase transformations were induced by acid addition and studied in the pH range 0.9–4.4 to monitor morphological changes and phase transformations using AFM, SEM and XRD.

2. Experimental

The dissolution of the synthetic manganite was studied both in short and long term experiments. For the short term experiments AFM, SEM and XRD was used to study morphological phase changes and identify the resulting phase. In the long term experiments proton consumption, redox potential and formation of aqueous Mn was monitored and the solid phases were analysed using XRD after 9, 12 and 17 months.

2.1. SOLUTIONS AND SUSPENSIONS

All solutions were made from deionised water (Milli-Q Plus 185). Stock solutions of HCl (Fisher, pro analysis) were standardized against tris(hydroxymethyl)aminomethane (Trizma base). NaOH (Merck, p.a.) solutions were then standardized against these stock HCl solutions. NaCl (Merck p.a., dried at 453 K) and $NaNO_3$ (Merck p.a., dried at 353 K) were used as ionic media. Solutions of Mn(II) for Atomic Absorption Spectroscopy standards were prepared through oxidation of Mn(s).

Manganite was synthesised and characterised according to Giovanoli and Leuenberger (1969) and Ramstedt et al. (2004) with XRD d-spacings of: 3.40, 2.64, 2.41, 2.27, 1.78, 1.70, 1.67 and 1.64 Å (See supplementary information). The size of the needle shaped manganite crystals were around 500 nm long and 20–40 nm wide. They have a pH_{iep} (pH of the iso electric point) of 8.2 in 10 mmol/dm^3 NaCl suspensions (Ramstedt et al., 2004). Surface areas were determined using the BET method (Brunauer, 1938). The samples used in the atomic force microscopy (AFM), scanning electron microscopy (SEM) and corresponding X-ray powder diffraction (XRD) analyses had surface areas of 39 m^2/g and were prepared from suspensions of 2–5 g of manganite/dm^3 and an ionic medium of 0.01 mol/dm^3 NaCl. In the long term dissolution studies for determining the apparent equilibrium constant, suspensions of 10 g of manganite (surface area of 48 m^2/g)/dm^3 was used and 0.1 mol/dm^3 $NaNO_3$ was used as the ionic medium.

2.2. BATCH EXPERIMENTS

2.2.1. *Long Term Experiments*

A calculation using the computer code WinSGW (available on the internet at http://www.chem.umu.se/dep/inorgchem/samarbeta/WinSGW_eng.stm and based on Eriksson, 1979) was performed for 10 g/dm^3 (0.114 mmoles/dm^3) of manganite. It was found that with pH $\leq$ 4.8 a complete transformation of γ-MnOOH(s) into β-MnO_2(s) and Mn^{2+} is obtained. Hence, the batch experiments performed in this study were designed to cover the range $5.0 \leq -\log [H^+] \leq 6.5$ in order to follow Mn(II) release, and $-\log [H^+]$ as a function of time. Furthermore, XRD patterns were collected at 9, 12 and 17 months to identify the solid phase(s) formed.

Manganite dissolution was studied by adding acid to test tubes containing solid suspensions. These samples were left to equilibrate on an end-to-end test tube rotator up to 17 months while $-\log [H^+]$ was measured in intervals of a few months using a combination electrode. No additional acid was added during these months. The concentration of H^+ was determined using Nernst equation (5);

$$E = E_0 + g \log[H^+] + E_j \tag{5}$$

where E is the potential in mV, E_0 is an apparatus constant determined separately, $g = \mathrm{RTln10/nF} = 59.16$ mV at 25 °C and $n = 1$. E_j is the liquid junction potential at the interface between electrode and the equilibrium solution. E_0 was determined from measurements of the potential in two diluted standardised H^+ solutions at 0.005 mol/dm^3 and 0.001 mol/dm^3. The redox potential in selected samples at 17 months was measured using a platinum redox electrode calibrated with a commercial redox standard (Orion ORP Standard by Thermo Electron Corporation) based on the equilibrium I^-/I_2.

The suspensions were sampled at 9, 12 and 17 months of reaction time. The samples aliquots were centrifuged and the solutions were filtered through 0.22 μm filters. The concentration of dissolved Mn in the solutions was determined using atomic absorbance spectrometry (AAS) on a Perkin-Elmer atomic absorption spectrometer 3110. The pastes were dried under reduced pressure and in presence of a drying agent (P_2O_5). After drying, the pastes were ground and analysed with XRD.

The XRD samples were measured using a Bruker D8 advance X-ray diffractometer in theta–theta mode with twin Göbel mirror parallel beam geometry, copper target tube operated at 40 kV and 40 mA. A 0.6 mm mirror housing exit slit was used on the incident beam, a 0.6 mm receiving slit and a 1° anti-scatter slit were used on the diffracted beam. Data was collected from 15.0° to 90.0° 2θ, with a step size of 0.01° 2θ, for 12 second per step. In

general the diffraction patterns were acquired on a rotating Si-plate during 24–48 hours. Diffraction peaks and mineral phases were identified in the X-ray diffractograms with the aid of Bruker Diffrac^{plus}Basic Evaluation Package, and the International Center for Diffraction Data (ICDD), Database, release 2004. The acquired diffraction patterns were relatively noisy and thus Fourier smoothing was applied as well as a background removal. The presence of a metal edge on the sample holder gave rise to a change in intensity in the diffraction patterns and made it impossible to acquire the diffraction pattern at $2\theta < 15°$ when the samples were rotated.

2.2.2. *Short Term Experiments*

The dissolution was studied by adding acid to test tubes containing solid suspensions. The samples were periodically shaken throughout the reaction period of a week and pH was measured using a combination electrode calibrated with commercial pH buffer solutions (MERCK). After 1 week the samples were centrifuged and the pastes were dried under reduced pressure and in presence of a drying agent (P_2O_5). After drying, the pastes were ground and analysed with XRD and SEM.

The SEM samples were covered with a 3 nm film of Ir metal using a Gatan ion beam coater, prior to measurements, and analysed on a Hitachi S5000 In-Lens Field Emission Scanning Electron Microscope equipped with both secondary electron and backscattered electron detectors. For each sample, 10–20 images were collected focusing especially on areas that displayed changes in morphology compared to the initial manganite crystals.

The XRD samples were measured using a Philips X′PERT X-ray diffractometer with a Bragg-Brentano parafocusing geometry and a long fine focus, copper target tube operated at 40 kV and 40 mA. A 1° divergence slit was used on the incident beam and a 0.3 mm receiving slit, a 1° anti-scatter slit and a graphite monochromator were used on the diffracted beam. Data was collected from 5.0° to 70.0° 2θ, with a step size of 0.02° 2θ, for 0.4 seconds per step. Samples were rotated during data collection. Diffraction peaks and mineral phases were identified in the X-ray diffraction patterns with the aid of XPLOT for Windows, Version 1.34, and the International Center for Diffraction Data (ICDD), Database Set 49.

AFM measurements were performed in order to obtain real-time images of the dissolving manganite crystals. A Nanoscope multimode AFM (Digital Instruments, Santa Barbara, US) was used operating in contact mode in an electrolyte solution using a standard cantilever with a V-shaped Si_3N_4-tip and a spring constant of approximately 0.3 N/m. The manganite crystals were adsorbed onto freshly cleaved mica by immersing the mica into a manganite suspension (5 g MnOOH/dm^3), lightly rinsing with water and mounting on a sample holder. After the first image of a separate crystal was obtained, a drop

of acid (0.01 mol/dm^3 HCl) was added and roughly one image per minute was collected to study the morphological changes of the crystals in real time. There was no control of pH during the experiment but the initial pH after addition of acid was around 2.5.

3. Results and Discussion

The mechanism for the dissolution of manganite is generally assumed to be through an energetically favourable disproportionation reaction (Giovanoli and Leuenberger, 1969; Klewicki and Morgan, 1999), which forms $Mn^{IV}O_2$ and Mn^{2+}-ions in solution. This disproportionation of manganite at low pH has previously been confirmed by XPS (Ramstedt et al., 2002).

3.1. MANGANITE DISPROPORTIONATION AT EQUILIBRIUM

From the incongruent disproportionation reaction (1), it is obvious that the phase transformation is favoured by a decreasing pH. A calculation using the computer code WinSGW was performed to illustrate the pH dependence of reaction (1) with the most stable MnO_2 phase, pyrolusite. The result of this calculation is visualized in Figure 2, and it is clear that the dissolution of manganite becomes significant at pH $\leq$ 6.

Experimental data of the batch experiments are given in Table I. It was found that the disproportionation process is quite slow. This was especially the case in the low pH range where almost complete phase transformation is to be expected. A calculation of log K(1) for each experimental point after 17 months resulted in $\log K^{0.1}(1) = 8.31 \pm 0.25$ (error = σ, I = 0.1 mol/dm^3). A recalculation to I = 0 using Davis equation resulted in $\log K^0(1) = 8.52 \pm 0.25$. Within the experimental errors, this value is the same as the one obtained by combining log $K^0(2)$ and log $K^0(3)$ given by Lindsay (1979) ($\log K^0(1) = 8.65$), but significantly higher than the one given by Klewecki and Morgan (1999), log K(1)$\approx$7.0. However the identity of the formed MnO_2 phase was not clearly stated in the latter study.

In the present study, a non-linear drift in the log $K^0(1)$ values was found with time (Table I). This could be indicative of a rearrangement of a meta-stable form of the solid MnO2 phase with time. It can be assumed that the initial disproportionation forms a mixed valence manganese oxide with a log $K^0(1)$ of 7.66 (12 months) which rearranges to form the more stable pyrolusite after 17 months with log $K^0(1)$ of 8.52. There is no direct evidence in XRD patterns of formation of birnessite or nsutite in these long term experiments. Birnessite is known to form very broad diffraction patterns with low intensity (Bricker, 1965) which would be difficult to observe in our diffraction patterns especially if present in low concentrations. However, it is

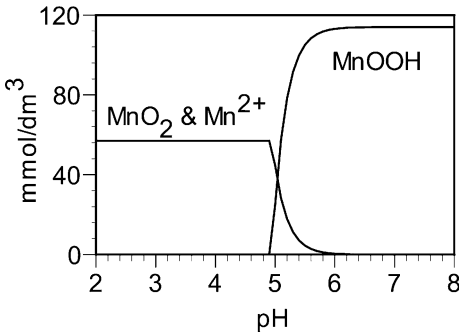

Figure 2. Plot showing the manganite dissolution at low pH and disproportionation to β-MnO_2 and Mn^{2+}-ions. The data in this plot were calculated for a 10 g/dm^3 suspension of manganite using the computer code WinSGW (Eriksson, 1979). In the calculation, log K(2) = 25.27 and log K(3) = 41.89 (Lindsay, 1979) were used.

very probable that these phases do form considering that log $K^0(1)$ is quite stable around 7.6 for several months before reaching its final value at 8.52. This hypothesis involving phase rearrangement also gives an explanation for the lower log $K^0(1)$ value reported by Klewicki and Morgan (1999).

The redox equilibrium (6) after 17 months was also investigated.

$$\beta\text{-}MnO_2(s) + H^+ + e^- \rightleftharpoons \gamma\text{-}MnOOH(s) \quad (6)$$

By plotting pH vs. pe, a slope close to −1 was obtained (-1.09 ± 0.01) (Figure 3) and calculations of the equilibrium constant gave a value of log $K^0 = 15.75 \pm 0.05$. A combination of log $K^0(1) = 8.52$ with log $K^0(6) = 15.75$ gives log $K^0(3) = 40.02$, a value close to the one (40.28) given by Ambrose et al. (1969) for highly crystalline and stoichiometric pyrolusite. This agreement indicates that microcrystalline particles of manganite favour a slow formation of highly crystalline pyrolusite particles. It is hypothesized that these pyrolusite particles are formed at the manganite surface, in agreement with the formation of crystalline surface precipitates in other metal (hydr)oxide systems (Gunneriusson and Sjöberg, 1993).

XRD measurements of the remaining solid phase in a sample with low pH (2.6) showed the transformation to pyrolusite (β-MnO_2) after 9 months (Figure 4). A comparison of the experimental equilibrium constants with literature values indicates that this reaction also takes place in the higher pH range, although the amount of $Mn^{IV}O_2$ would be too low to be detectable in XRD. May be this also gives an explanation for the frequent absence of pyrolusite formation in laboratory experiments although it is the normal end product in the environment (Bricker, 1965). However, the presence of an amorphous or highly disordered $Mn^{IV}O_2$ phase is also possible and might not be possible to distinguish in our diffraction patterns.

Table I. The concentration of manganese and protons together with log K^0 values after 9, 12 and 17 months (m) of reaction time

9 m			12 m			17 m				
log $[H^+]$	log $[Mn^{2+}]$	log$K^0(1)$	log $[H^+]$	log $[Mn^{2+}]$	log $K^0(1)$	log $[H^+]$	log $[Mn^{2+}]$	log $K^0(1)$	pe	log $K^0(6)$
−6.80	−6.22	7.59	−6.75	−6.08	7.64	−6.96	−5.76	8.37		
−6.25	−4.86	7.84	−5.96	−4.15	7.98	−6.41	−4.07	8.96	9.19	15.71
−5.87	−4.09	7.85	−5.54	−3.51	7.78	−5.88	−3.45	8.51	9.78	15.77
−5.43	−3.58	7.49	−5.40	−3.33	7.68	−5.73	−3.33	8.34	9.85	15.69
−5.30	−3.39	7.43	−5.30	−3.24	7.56	−5.65	−3.22	8.29		
−5.21	−3.26	7.38	−5.22	−3.36	7.30	−5.63	−2.83	8.63	10.09	15.82
Average		7.60			7.66			8.52		15.75
Standard deviation		0.21			0.23			0.25		0.05

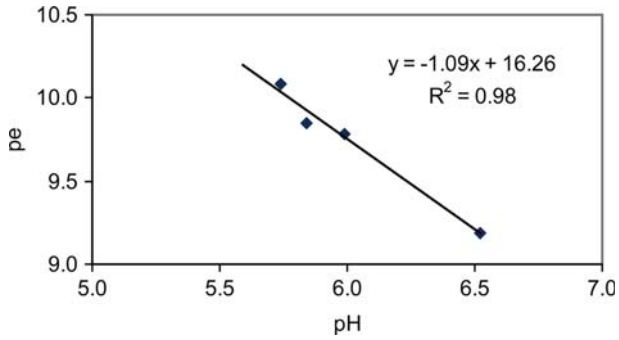

Figure 3. Plot of pe vs. pH showing the 1:1 ratio and the logarithm of the equilibrium constant for Equation (6).

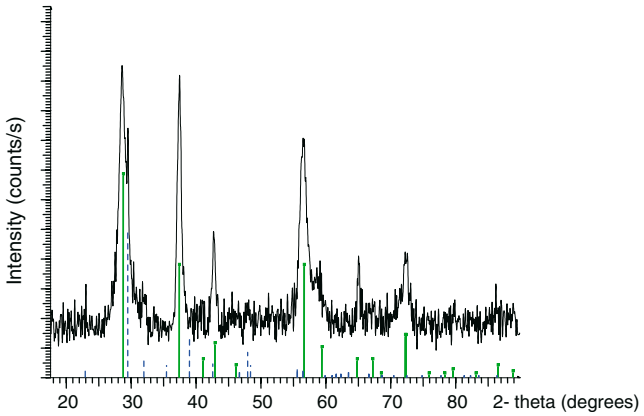

Figure 4. XRD patterns of a batch sample at pH 2.6 showing that parts of the manganite has transformed into pyrolusite (literature values represented by the solid lines). The presence of $NaNO_3$ from the ionic medium is represented by broken lines. The broadening of the peaks is most likely due to the small crystal sizes.

3.2. NON-EQUILIBRIUM MEASUREMENTS

The morphological changes occurring during the dissolution of crystals can sometimes give an insight into the difference in reactivity between the different surfaces on a mineral crystal. To study this, real-time AFM measurements were performed on dissolving manganite particles. It was found that the largest visual changes were observed at the edges of the crystals. After 2 hours of dissolution, shortening of the needles was observed while the width was more or less maintained, as seen in Figure 5.

The images in Figure 5 could indicate that the reactive part of the crystals, with respect to dissolution, is not primarily the basal planes of the crystals but the comparably smaller area represented by the edges. It should be noted, though, that the dissolution of the basal plane would not give the same visual effect as the dissolution of the small areas that form the edges. From the AFM images, no separate phase was identified that could be interpreted as a Mn(IV) oxide. Instead, the crystal structure has to rearrange internally (as previously suggested by Giovanoli and Leuenberger, 1969). Alternatively the Mn(IV) phase is precipitated evenly on the manganite or mica surface, or is swept away from the field of view by the AFM tip. From the AFM images a rough estimate of the dissolution rate can be performed, although one should keep in mind that the mechanical rastering of the AFM tip over the crystal might enhance the dissolution slightly. Assuming a cylindrical geometry, the volume change during dissolution was calculated from the images and resulted in a 22% volume reduction during the first 2 hours. However, this rate should only be considered as an initial rate since the dissolution rate seems to decrease with time.

The shortening of the manganite needles observed in AFM, could also be seen in SEM images. However, in SEM images the needles also appear to become more flattened, indicating that the larger basal planes actually do participate in the extended (1 week) dissolution process (Figure 6). Furthermore, a secondary phase was observed with decreasing pH (after 1 week of reaction time). In the images from pH $\leq$ 3.8 a fraction of needles, with smaller dimensions than manganite, can be observed in addition to the manganite crystals, although the dominating morphology in all the samples was the manganite crystals. The tiny needles are assumed to be the newly formed Mn(IV) phase but could also be smaller manganite particles. Since

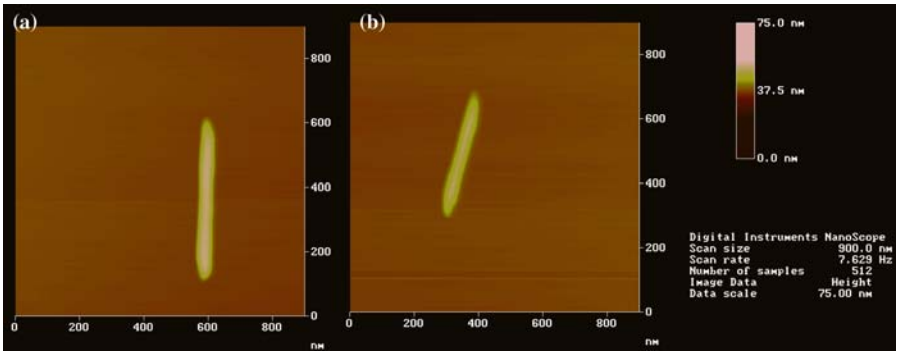

Figure 5. Real time AFM images of a dissolving manganite crystal. Image (a) before the addition of acid and image (b) is recorded after approximately 120 minutes reaction time. The scale bar in the upper right corner of the image shows the height of the crystals.

the pyrolusite is known to form needle shaped crystals (Berry, 1983; Varentsov and Grassely, 1980) it would be difficult to differentiate between these two phases, but it is likely that the newly formed MnO_2 phase would have a smaller particle size and exist in smaller quantities, as is the case for the new phase observed in the SEM images.

XRD patterns of the samples were difficult to interpret as a consequence of the overlap between reflections from different manganese oxides (Table II). Furthermore, the identification of the new phases was challenging due to their low concentration and the small sizes of the crystals, which result in a broadening of the peaks.

Despite these problems, the XRD patterns suggest the presence of a new phase, ramsdellite, with a reflection at ~4.1 Å at pH 3.8 (Figure 7) although this reflection could also come from a nsutite mineral phase. The reflection do not have a high intensity but is clearly absent in the diffraction patterns for

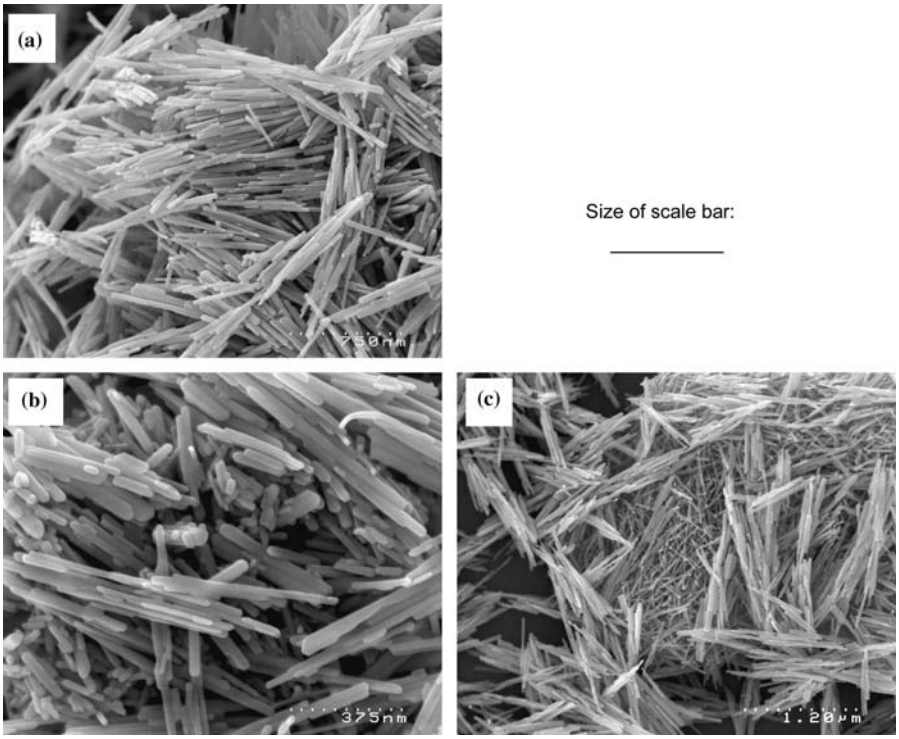

Figure 6. Image (a) shows manganite crystals at pH 4.4. Image (b) is of parts of the solid phase at pH 3.8 showing the short and flat remains of the manganite crystals. Image (c) shows the fraction of tiny needles formed at pH ≤ 3.8 (centre of image). The larger crystals in (c) are manganite. All images were collected after one week of reaction time, and the samples were dominated by manganite crystals throughout the pH range studied. The scale bar represents (a) 750 nm (b) 375 nm (c) 1.20 μm.

Table II. Literature d-values (ICDD, 1997) in Å (relative intensities in %) for a selected range of solid phases

Phase	Identification[a]	Overlap 1[a]	Overlap 2[a]
Ramsdellite	4.06 (100)	2.55 (38), 2.34 (31), 2.43 (29), 1.65 (20)	2.14 (19)
Nsutite	4.00 (95)	1.64 (100), 2.33 (70), 2.42 (65), 1.60 (45), 1.37(40)	2.13 (45)
Pyrolusite	3.11 (100), 2.11 (16)	2.41 (55), 1.62 (55), 1.30 (20 + 20)	
$MnCl_2$	5.64 (100), 4.40 (65), 2.79 (45), 2.92 (25),	2.42 (25)	2.82 (30), 2.12 (20)
NaCl	1.99 (55)		2.82 (100),
$NaNO_3$	3.04 (100), 1.90 (17), 2.81 (14),	2.31 (26)	
$Mn(NO_3)_2$	4.14 (100), 5.77 (85), 2.74 (75), 4.94 (50)	4.82 (60), 3.39 (45), 2.41 (40)	

[a]Identification = reflections possible to use for identification.
Overlap 1 = reflections that can overlap with manganite reflections.
Overlap 2 = reflections that can overlap with other manganese oxides or NaCl.

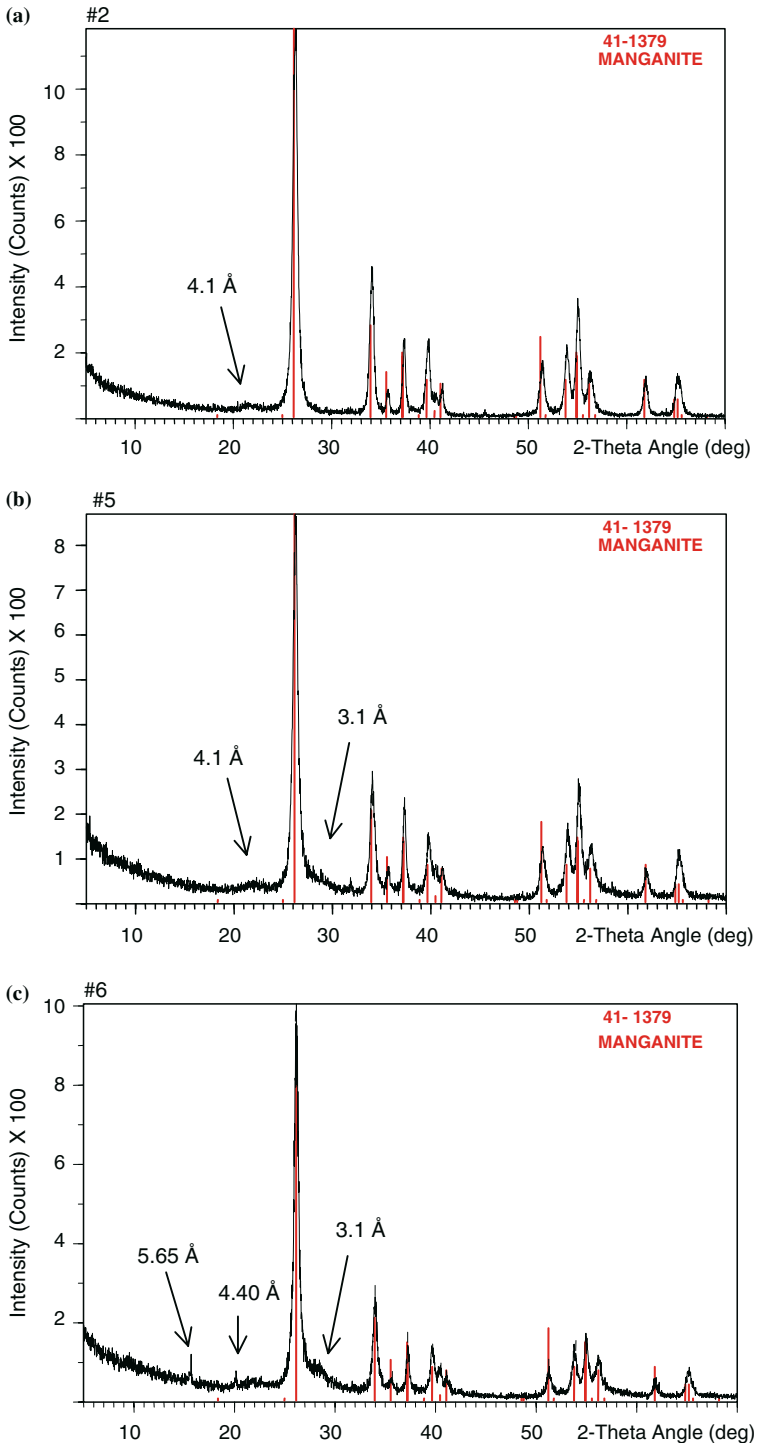
(a)
#2
41-1379
MANGANITE
Intensity (Counts) X 100
4.1 Å
2-Theta Angle (deg)
(b)
#5
41- 1379
MANGANITE
Intensity (Counts) X 100
4.1 Å
3.1 Å
2-Theta Angle (deg)
(c)
#6
41- 1379
MANGANITE
Intensity (Counts) X 100
5.65 Å
4.40 Å
3.1 Å
2-Theta Angle (deg)

Figure 7. XRD patterns of manganite at (a) pH 3.8, (b) 1.6 and (c) 0.9. The positions for the manganite reflections are marked in the diffraction patterns by solid lines (ICDD, 1997). The indications for ramsdellite at 4.1 Å, pyrolusite at 3.1 Å and $MnCl_2$ at 5.65 and 4.40 Å is marked by arrows in the figures.

the pure manganite phase (see supplementary information). This reflection is present in all the diffraction patterns at pH ≤ 3.8 and grows slightly with decreasing pH. This coincides with the morphologically different phase observed in the SEM pictures at these pH levels and suggest that the fraction of tiny needles found in SEM images are ramsdellite (Varentsov and Grassely, 1980). This phase is often described as $MnO_{x<2}$ where x is 1.97 (Gattow and Glemser, 1961; Varentsov and Grassely, 1980).

In the diffraction patterns at pH 1.6 and 0.9 (Figure 7), a shoulder (at 3.1 Å) on the main manganite peak (at 3.4 Å) was formed. This shoulder indicates the formation of pyrolusite in the lowest pH range. This new phase was not recognised in the SEM images, which could indicate that the formation of pyrolusite occurs through rearrangement of the manganite or ramsdellite phases. However, this phase could also be present in too small amounts to be observed in the SEM images or have morphology similar to the other phases present.

The experiments with one week of reaction time only dissolved parts of the manganite. But, as previously described, manganite was observed to rearrange into pyrolusite at pH < 2.6 if longer equilibration times were allowed. The presence of layered MnO_2 phases could not be evidenced but also not disproved in this study, thus, the presence of such a phase remains an open question. However, the rearrangement of manganite to pyrolusite is in agreement with literature observations (Kohler et al., 1997; Yamada and Ohmasa, 1986), describing the formation of a mixture of pyrolusite and ramsdellite in solid state oxidation of manganite. Although the present study is performed in solution, similar mechanisms can be expected to take place. This assumption is also supported by the long time dissolution experiments which indicate that a manganese oxide with lower valence than four is initially formed and then transformed into pyrolusite.

In SEM images from a sample at pH 1.6, hexagonal platelets were found (Figure 8). These platelets have the same morphology as large $MnCl_2 \times 4H_2O$ crystals, which suggests that they are a precipitate falling out of solution during the drying procedure before the XRD. This precipitate was also observed in XRD patterns at the lowest pH. Furthermore, a NaCl precipitate (ionic medium) was observed in XRD patterns from samples at higher pH (Table III). The reason for the occurrence of these $MnCl_2$ platelets would be the relatively high concentrations of Mn^{2+} and Cl^- at the lowest pH values and the absence of the platelets in the

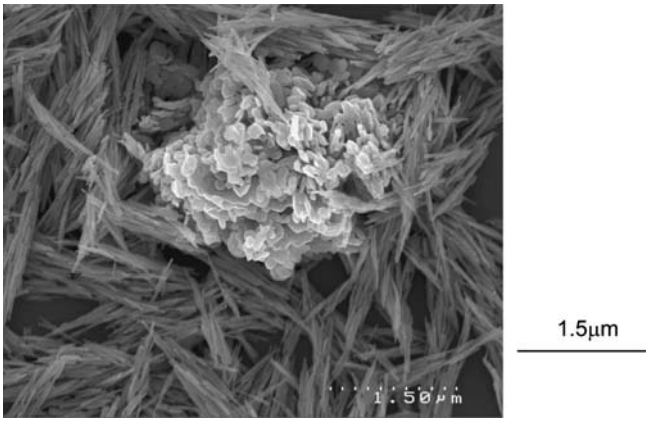

Figure 8. SEM image showing parts of the remaining solid phase after one week, pH 1.6. The needles are manganite and the platelets are assumed to be a $MnCl_2$ precipitate from solution. The scale bar represents 1.5 µm.

Table III. Solid phases identified from XRD patterns and SEM pictures after one week reaction time

pH	*XRD pattern*	*XRD*	*SEM*	*MnOOH* (g/dm^3)
4.4		Manganite	Manganite	5
3.8	Figure 7a	Manganite	Manganite	5
		Ramsdellite	Small needles	
		NaCl		
3.1		Manganite	Manganite	2
		Ramsdellite	Small needles	
		NaCl		
2.9		Manganite	Manganite	2
		Small needles		
1.6	Figure 7b	Manganite	Manganite	5
		Ramsdellite	Small needles	
		Pyrolusite	Hexagons	
0.9	Figure 7c	Manganite		2
		Ramsdellite	Manganite	
		Pyrolusite	Small needles	
		$MnCl_2$		

XRD solid phases indicated in XRD patterns.
SEM separate phases observed in SEM pictures.

SEM images at the lowest pH is probably due to that the dried sample is slightly inhomogeneous and a larger sample size should have been analysed.

4. Conclusions

The dissolution of manganite at pH < 6.5 was observed to form β-MnO_2 in the prolonged dissolution (after 17 months), through the following disproportionation reaction:

$$2\gamma\text{-MnOOH(s)} + 2H^+ \rightleftharpoons \beta\text{-}MnO_2\text{(s)} + Mn^{2+} + 2H_2O,$$
$$\log K^0 = 8.52 \pm 0.25$$

This pyrolusite mineral was hypothesized to be formed by reconstruction of previously formed $Mn^{IV}O_2$ phases such as ramsdellite and/or nsutite. The presence of a layered MnO_2 phase could neither be proven nor excluded in the present study. In a shorter time span (1 week), XRD patterns and SEM images indicated the presence of ramsdellite and pyrolusite depending on pH of the suspension, again suggesting that non-equilibrium dissolution processes initially produce ramsdellite but that this phase rearranges with time to form β-MnO_2. From AFM measurements, the onset of dissolution was identified primarily at the short apices of the manganite crystals, and in SEM images after one week this initial dissolution was followed by flattening of the manganite needles.

Acknowledgements

The authors would like to acknowledge Ewen Silvester, Michael Horne and Nicki Agron-Olshina at CSIRO Minerals, Melbourne Australia for providing lab space and providing their skills in geochemistry, SEM and XRD. Patrick Hartley and Celesta Fong, at CSIRO Molecular Sciences, Melbourne Australia, are acknowledged for their help with the AFM measurements and for providing desk space for MR. Furthermore Dan Boström, Department of Chemistry, Umeå University is acknowledged for help with further XRD measurements. The authors would also like to thank three anonymous referees for their insightful comments on the manuscript. This work was supported by the Swedish Research Council.

References

Ambrose J., Covington A. K. and Thirsk H. R. (1969) Standard electrode potential of β-Manganese Dioxide and its relation to other properties. *Trans. Faraday Soc.* **65**, 1897–1905.

Amouric M., Parc S. and Nahon D. (1991) High resolution transmission electron microscopy study of Mn-hydroxide transformations and accompanying phases in a lateric profile of Moanda, Gabon. *Clays and Clay Minerals* **39**(3), 254–263.

Berry L. G. and Mason B. (1983) *Mineralogy – Concepts, Descriptions, Determinations*, 2nd Edn. (ed. R. V. Dietrich), W. H. Freeman and Company, San Fransisco.

Bochatay L., Persson P. and Sjöberg S. (2000) Metal ion coordination at the water-manganite (γ-MnOOH) interface I. An EXAFS study of Cadmium(II). *J. Colloid Interface Sci.* **229**, 584–592.

Bricker O. (1965) Some stability relations in the system $Mn–O_2–H_2O$ at 25° and one atmosphere total pressure. *Am. Mineral.* **50**, 1296–1354.

Brunauer S., Emmett P. H. and Teller E. (1938) Adsorption of gases in multimolecular layers. *J. Am. Chem. Soc.* **60**, 309–319.

Chabre Y. and Pannetier J. (1995) Structural and electrochemical properties of the proton/γ-MnO_2 system. *Prog. Solid. St. Chem.* **23**, 1–130.

Chiu van Q. and Hering J. G. (2000) Arsenic adsorption and oxidation at manganite surfaces. 1. Method for simultaneous determination of adsorbed and dissolved arsenic species. *Environ. Sci. Technol.* **34**, 2029–2034.

Eriksson G. (1979) An algorithm for the computation of aqueous multi-component, multiphase equilibria. *Anal. Chim. Acta* **112**, 375–383. http://www.chem.umu.se/dep/inorgchem/samarbeta/WinSGW_eng.stm.

Gattow von G. and Glemser O. (1961) Darstellung und Eigenschaften von Braunsteinen. III (Die ε-, β-, und α-Gruppe der Braunsteine, über Ramsdellit und über die Umwandlungen der Braunsteine. *Z. Anorg. Allg. Chemie.* **309**, 121–150.

Giovanoli R. and Leuenberger U. (1969) Über die oxidation von manganoxidhydroxide. *Helv. Chim. Acta* **52**, 2333–2347.

Gunneriusson L. and Sjöberg S. (1993) Surface complexation in the H^+-Goethite (α-FeOOH)-Hg(II)-chloride system. *J. Colloid Interface Sci.* **156**, 121–128.

Hem J. D. and Lind C. J. (1983) Nonequilibrium models for predicting forms of precipitated manganese oxides. *Geochim. Cosmochim. Acta* **47**, 2037–2046.

Högfeldt E. (1982) *Stability Constants of Metal-ion Complexes – Part A: Inorganic Ligands*. Pergamon Press, Oxford, England.

ICDD International Centre for Diffraction Data (1997) *Powder Diffraction File*. Pennsylvania, USA.

Johnson C. A. and Xyla A. G. (1991) The oxidation of chromium(III) to chromium(VI) on the surface of manganite (γ-MnOOH). *Geochim. Cosmochim. Acta* **55**, 2861–2866.

Klewicki J. K. and Morgan J. J. (1999) Dissolution of β-MnOOH particles by ligands: Pyrophosphate, etylenediaminetetraacetate, and citrate. *Geochim. Cosmochim. Acta* **63**, 3017–3024.

Kohler T., Armbruster T. and Libowitzky E. (1997) Hydrogen bonding and Jahn-Teller distortion in Groutite, α-MnOOH, and Manganite, γ-MnOOH, and their relations to the manganese dioxides ramsdellite and pyrolusite. *J. Solid St. Chem.* **133**, 486–500.

Lindsay W. L. (1979) *Chemical Equilibria in Soils*. John Wiley and Sons, New York.

Manceau A., Drits V. A., Silvester E., Bartoli C. and Lanson B. (1997) Structural mechanism of Co^{2+} oxidation by the phyllomanganate buserite. *Am. Mineral.* **82**, 1150–1175.

Mcardell C. S., Stone A. T. and Tian J. (1998) Reaction of EDTA and realted aminocarboxylate chelating agents with $Co^{III}OOH$ (Heterogenite) and $Mn^{III}OOH$ (Manganite). *Environ. Sci.Technol.* **32**, 2923–2930.

Murray J. W., Dillard J. G., Giovanoli R., Moers H. and Stumm W. (1985) Oxidation of Mn(II): Initial mineralogy, oxidation state and ageing. *Geochim. Cosmochim. Acta* **49**, 463–470.

Nico P. S. and Zasoski R. J. (2001) Mn(III) center availability as a rate controlling factor in the oxidation of phenol and sulphide on δ-MnO_2. *Environ. Sci. Technol.* **35**, 3338–3343.

Post J. E. (1999) Manganese Oxide minerals: Crystal structures and economic and environmental significance. *Proc. Natl. Acad. Sci. USA* **96**, 3447–3453.

Ramstedt M., Shchukarev A. and Sjöberg S. (2002) Characterization of hydrous manganite (γ-MnOOH) surfaces – an XPS study. *Surf. Interface Anal.* **34**, 632–636.

Ramstedt M., Andersson B., Shchukarev A. and Sjöberg S. (2004) Surface properties of hydrous manganite (γ-MnOOH) – a potentiometric, electroacoustic and XPS study. *Langmuir* **20**, 8224–8229.

Shaughnessy D. A., Nitsche H., Booth C. H., Shuh D. K., Waychunas G. A., Wilson R. E., Gill H., Cantrell K. J. and Serne R. J. (2003) Molecular interfacial reactions between Pu(VI) and Manganese Oxide minerals Manganite and Hausmannite. *Environ. Sci. Technol.* **37**, 3367–3374.

Sillén L. G. and Martell A. E. (1971) *Stability Constants of Metal-ion Complexes Spec Publ. 25*. The Chemical Society, London.

Stumm W. and Giovanoli R. (1976) On the nature of particulate manganese in simulated lake waters. *Chimica* **30**(6), 423–425.

Varentsov I. M. and Grassely G. Y. (1980) *Geology and Geochemistry of Manganese, Volume 1*. E. Schweizerbart'she Verlagsbuchhandlung, Stuttgart, Germany.

Weaver R. M., Hochella M. F. and Ilton E. S. Jr. (2002) Dynamic processes occurring at the Cr^{III}_{aq}-manganite (γ-MnOOH) interface: Simultaneous adsorption, microprecipitation, oxidation/reduction and dissolution. *Geochim. Cosmochim. Acta* **66**, 4119–4132.

Xyla A. G., Sulzberger B., Luther G. W. III., Hering J. G., Van Cappellen P. and Stumm W. (1992) Reductive dissolution of the manganese(III,IV) (Hydr)oxides by oxalate: The effect of pH and light. *Langmuir* **8**(1), 95–103.

Yamada N. and Ohmasa M. (1986) Textures in natural pyrolusite, β-MnO_2, examined by 1 MV HRTEM. *Acta Cryst.* **B42**, 58–61.